ISSN 1063-7710, Acoustical Physics, 2011, Vol. 57, No. 1, pp. 1–9. © Pleiades Publishing, Ltd., 2011.
Original Russian Text © V.G. Andreev, T.B. Krit, V.V. Kostikov, A.V. Shanin, S.I. Shinderuk, 2011, published in Akusticheskiĭ Zhurnal, 2011, Vol. 57, No. 1, pp. 3–12.

CLASSICAL PROBLEMS OF LINEAR ACOUSTICS AND WAVE THEORY

Shear Standing Waves in a Resonator with a Rubberlike Inhomogeneous Medium

V. G. Andreev, T. B. Krit, V. V. Kostikov, A. V. Shanin, and S. I. Shinderuk

Faculty of Physics, Moscow State University, Moscow, 119991 Russia

e-mail: timofey@acs366.phys.msu.ru

Received July 29, 2010

Abstract—A modification of the finite-element method is proposed for calculating shear standing waves in a resonator filled with an incompressible elastic medium with allowance for the finite dimensions of the resonator and inhomogeneities of the shear modulus. Resonance curves are calculated for resonators with inhomogeneities in the form of cavities and elastic inclusions. Numerical calculations are compared with experimental data.

DOI: 10.1134/S1063771011010027

INTRODUCTION

Earlier [1], we studied shear waves in a one-dimensional resonator that had the form of a layer of a homogeneous rubberlike medium the upper surface of which had a finite-mass plate attached to it while the lower surface performed harmonic vibrations with a preset acceleration. We showed (both theoretically and experimentally) that, in such a system, resonances occur at frequencies the values of which depend on the mass of the upper plate and the shear modulus of the layer. From the measured resonance curves, we determined the shear modulus and the shear viscosity coefficient of the rubberlike material in the low-frequency range. In [2], we used a one-dimensional model to analyze standing waves in a resonator filled with a medium the shear modulus of which varied in the direction perpendicular to shear displacements.

In this paper, we study wave processes in a finite-size resonator with different types of inhomogeneities of the shear modulus. The resonator has the form of a parallelepiped made from rubberlike material and fixed without slippage to a horizontal plate. The upper face of the parallelepiped is either free or loaded with a finite-mass plate. Simulation is performed by the finite-element method (FEM) [3].

THE FINITE-ELEMENT METHOD FOR AN INCOMPRESSIBLE RUBBERLIKE MEDIUM

Let x_i represent the coordinates of resonator particles before deformation and u_i represent the particle displacements due to deformation. In the linear approximation, deformation is described by the strain tensor $\varepsilon_{ij} = \frac{1}{2}(u_{i,j} + u_{j,i})$, where $u_{i,j} = \frac{\partial u_i}{\partial x_j}$, and $i, j = 1, 2, 3$. The internal stresses caused by deformation are described by the stress tensor σ_{ij}. The equation of motion has the form

$$\rho\ddot{u}_i = \sigma_{ij,j} + b_i, \tag{1}$$

where $\sigma_{ij,j} = \frac{\partial \sigma_{ij}}{\partial x_j}$, $i, j = 1, 2, 3$, ρ is the density of the material and b_i is the external bulk force. The stress–strain relation is given by the formula

$$\sigma_{ij} = \lambda\varepsilon_{kk}\delta_{ij} + 2\mu\varepsilon_{ij} + 2\eta\dot{\varepsilon}_{ij}, \tag{2}$$

where λ and μ are the Lamé coefficients and η is the shear viscosity coefficient.

We apply the finite-element method by using the classical approach [4]. Below, we describe the main steps of the method.

A parallelepiped with a thickness L, a length a, and a width b was divided into finite elements in the form of triangular prisms (Fig. 1a). The size of the prisms was chosen so that the error in determining the resonance frequencies was within 1%, which agreed with the experimental conditions. In this case, the optimal way of dividing the parallelepiped was as follows: 5–10 elements in thickness, 10–15 elements in length, and 4–6 elements in width. A decrease in the size of finite elements, especially those near the vertices of the layer and the inhomogeneities, allows more accurate calculation of the resonance characteristics by the proposed method. However, the decrease in the finite element size leads to an increase in the computer time required for determining the resonance characteristics.

Let us consider the unit triangular prism shown in the inset in Fig. 1a. The nodes of the prism are numbered from 1 to 6. The bases formed by the nodes 1–2–3 and 4–5–6 have the form of right-angle triangles. In calculating the elementary matrices for a prism of

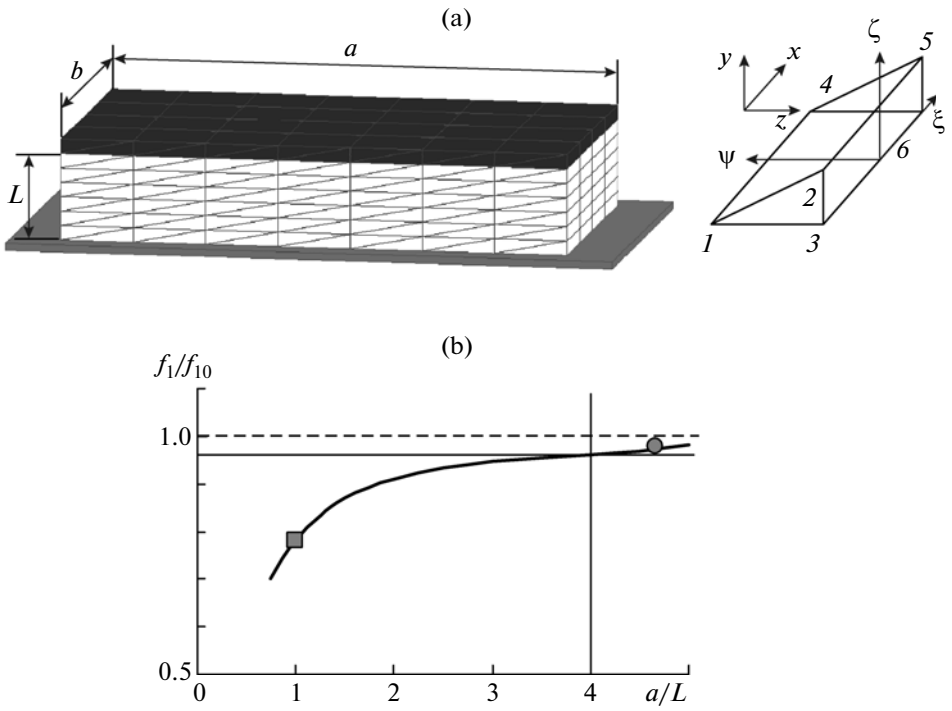

Fig. 1. (a) Scheme of the finite-element method. (b) Dependence of the first resonance frequency on the ratio of the resonator length to the resonator thickness. The horizontal solid line indicates the ratio $f_1/f_{10} = 0.96$, where f_{10} is the resonance frequency calculated using the one-dimensional model. The dots show the experimental data: the full circle corresponds to a resonator with $a/L = 4.7$, and the full square to a resonator in the form of a cube ($a/L = 1$).

arbitrary size, we use mapping of the actual prism onto the unit one. For the coordinates of the unit prism (ξ,ψ,ζ), we use the term "natural" (or "local") coordinates of the element, as distinct from the global coordinates (x,y,z).

Let the values of a certain function $\Phi(\xi,\psi,\zeta)$ be preset at the nodes of the prism. Then, the values of Φ at the points inside the prism can be calculated by interpolation:

$$\Phi(\xi,\psi,\zeta) = \sum_{i=1}^{6} \Phi_i N_i(\xi,\psi,\zeta), \tag{3}$$

where Φ_i is the value of Φ at the ith node and $N_i(\xi,\psi,\zeta)$ are the interpolation functions [3].

To map an arbitrary prism onto the unit one, we use Eq. (3) with the function $[\Phi]$ being sequentially set identical to x, y, and z. For simplicity, we assume that the nodes 1–2–3 lie in the yz plane. Then, the coordinate transformation formulas are simplified:

$$\begin{cases} x = x_1\dfrac{1-\xi}{2} + x_4\dfrac{1+\xi}{2}, \\ y = y_1\psi + y_2\zeta + y_3(1-\psi-\zeta), \\ z = z_1\psi + z_2\zeta + z_3(1-\psi-\zeta). \end{cases} \tag{4}$$

The determinant of the Jacobian matrix of transformation (4) is

$$\det J = \frac{1}{2}x_{41}(y_{13}z_{23} - y_{23}z_{13}), \tag{5}$$

where $x_{ij} = x_i - x_j$, $y_{ij} = y_i - y_j$, and $z_{ij} = z_i - z_j$. Note that the value of expression (5) is identical to the prism volume V.

If a rigid plate with a finite mass is attached to the upper boundary of the parallelepiped, one more row of triangular prisms is added to the layer thickness (the upper row in Fig. 1a). The prisms of this row are characterized by the Lamé coefficients and the shear viscosity coefficient of the upper plate material. The density of the prisms is calculated as the ratio of the mass of the upper plate to the volume of the added row. In fact, this corresponds to a resonator in the form of a two-layer structure fixed to a horizontal plate. Thus, the proposed method also allows one to study shear standing waves in a resonator that has the form of a structure consisting of parallel layers with plane interfaces [2].

We divide the parallelepiped boundary Γ into two nonintersecting parts: Γ_u and Γ_t. The part Γ_u corresponds to the lower boundary fixed to the plate, and the part Γ_t to the rest of the boundary. For the part Γ_u, the displacements of its points $\hat{u}_i$ are preset, whereas,

for the part Γ_t, we have a preset external surface stress $\hat{t}_i$. Then, the boundary conditions have the form

$$u_i|_{\Gamma_u} = \hat{u}_i = A\sin 2\pi ft, \quad (6)$$

$$\sigma_{ij}n_j|_{\Gamma_t} = \hat{t}_i = 0, \quad (7)$$

where f is the frequency of vibrations. Condition (6) corresponds to the displacement of the lower boundary according to the harmonic law with the frequency f and a preset amplitude A. Condition (7) means that all the other boundaries of the parallelepiped are free; i.e., the external stresses at these boundaries are zero. Condition (7) is also valid for a resonator with a loaded upper boundary of the layer, because, in this case, the upper boundary of the plate attached to the layer is still free.

We multiply Eq. (1) by an arbitrary function δu_i that is zero within the boundary region Γ_u; then, we perform integration over the entire volume Ω:

$$\int_\Omega \delta u_i(\rho\ddot{u}_i - \sigma_{ij,j} - b_i)d\Omega = 0.$$

As a result of integration by parts, we arrive at the expression

$$\int_\Omega \delta u_i\sigma_{ij,j}d\Omega = \int_\Omega (\delta u_i\sigma_{ij})d\Omega - \int_\Omega \delta u_{i,j}\sigma_{ij}d\Omega,$$

where the first term on the right-hand side is zero. Indeed, according to the Ostrogradski–Gauss theorem, this term is transformed to the integral over the closed surface Γ bounding the volume Ω. Taking into account Eq. (7) and the fact that $\delta u_i = 0$ at the boundary part Γ_u, we obtain that this integral is zero. Finally, we obtain the expression of the virtual work principle,

$$\int_\Omega \delta u_i\rho\ddot{u}_i d\Omega + \int_\Omega (\delta\varepsilon_{ij}\sigma_{ij})d\Omega - \int_\Omega \delta u_i b_i d\Omega = 0, \quad (8)$$

where $\delta\varepsilon_{ij} = \frac{1}{2}(\delta u_{i,j} + \delta u_{j,i})$.

To apply the FEM to solving Eq. (8), we divide the entire volume Ω into prisms with volumes Ω^e and separate the integrals involved in Eq. (8) into sums of integrals over the elements. Specifically, for each of the prisms, we represent Eq. (2) in the form

$$\sigma = E\varepsilon + G\dot{\varepsilon}, \quad (9)$$

where E and G are the elastic modulus matrix and the viscosity coefficient matrix, respectively.

Here, the symmetric tensors σ and ε are represented in the form of six-dimensional vectors. The first three components correspond to the pairs of indices xx, yy, and zz, and the last three components to the pairs of indices xy, xz, and yz. This vector representation is convenient and, therefore, widely used for computations in the theory of elasticity.

The change from the strain vector of the prism to its particle displacement vector is performed according to the formula $\varepsilon = Su$, where $u = [u_x, u_y, u_z]^T$ is the displacement vector and S is the symmetric gradient operator:

$$S = \begin{pmatrix} \frac{\partial}{\partial x} & 0 & 0 & \frac{\partial}{\partial y} & \frac{\partial}{\partial z} & 0 \\ 0 & \frac{\partial}{\partial y} & 0 & \frac{\partial}{\partial x} & 0 & \frac{\partial}{\partial z} \\ 0 & 0 & \frac{\partial}{\partial z} & 0 & \frac{\partial}{\partial x} & \frac{\partial}{\partial y} \end{pmatrix}^T.$$

At every point, the displacement vector components are related to the components of the node displacement vector according to Eq. (3). Finally, we obtain $\varepsilon = SNU \equiv BU$, where U is the node displacement vector and N is the interpolation function matrix. Then, Eq. (9) takes the form $\sigma = BEU + BG\dot{U}$.

The mass matrix of a single prism is determined as

$$M^e = \rho\int_{\Omega^e} N^T(x,y,z)N(x,y,z)dxdydz$$
$$= \rho V\int_\varpi N^T(\xi,\psi,\zeta)N(\xi,\psi,\zeta)d\xi d\psi d\zeta.$$

The integral over $\varpi = \{(\xi,\psi,\zeta) : -1 \le \xi \le 1; 0 \le \psi \le 1; 0 \le \zeta \le 1-\psi\}$ is determined by the form of the interpolation functions alone and does not vary from one element to another.

When applied to the problems of strain calculation in incompressible media, the standard FEM exhibits a considerable disadvantage, which is called the volumetric locking [3, 4]. In the standard FEM, the incompressibility condition is expressed as the condition of volume conservation for each of the prisms. This leads to an excessive number of constraints in comparison with the number of the degrees of freedom of the system obtained by discretization of the continuous displacement field. The stiffness of the grid becomes higher than that of the actual material, and the strain calculated by the FEM proves to be smaller than the actual one. The influence of the ratio of the number of degrees of freedom to the number of nodes on the deformation of an incompressible medium was analyzed in [5]. It was shown that, when this ratio is unity or smaller, volume blocking takes place. For example, in the case of a plane region divided into triangles, the number of triangles is almost twice as great as the number of nodes (accurate to the number of nodes at the boundary of the region). At the same time, the number of degrees of freedom is precisely twice as great as the number of nodes (the node displacements occur in two coordinates). If the areas of the triangles are fixed, the number of the remaining degrees of freedom is on the order of the number of nodes at the boundary, which is insufficient for describing the strain of the body. In practice, this leads to the appearance of "easy" and "hard" directions of

shear strain, with the situation not changing as the grid grows finer (i.e., no convergence takes place). Therefore, in our study, we use a modified FEM, namely, a method in which the volume variations are averaged over the nodes [6]. In this method, we determine not the volume of each individual finite element, but the average volume pertaining to each of the nodes. Thus, the number of the degrees of freedom used in the calculations is identical to the number of nodes, which allows us to adequately describe the strain of a rubber-like body.

To take into account the incompressibility, we used the following algorithm of calculating the rigidity of the system. The shear and bulk rigidities are calculated separately.

Assuming that $\lambda = 0$, we determine the shear rigidity matrix. It is expressed through the integral

$$K_t^e = \int_{\Omega^e} B^T(x,y,z)E(x,y,z)B(x,y,z)dxdydz,$$

which is calculated in the same way as described above.

The bulk rigidity matrix is determined at each of the vertices as the average matrix over the group of elements with a given vertex. For this purpose, we find the average bulk strain of the group of elements adjacent to the given vertex:

$$\langle \varepsilon_v \rangle = \frac{1}{V}\int_{\Omega} \varepsilon_v d\Omega = \frac{1}{V}\sum_e \int_{\Omega^e} \varepsilon_v d\Omega = \sum_e \frac{V_e}{V}\left\langle \varepsilon_v^e \right\rangle = \sum_e w^e \left\langle \varepsilon_v^e \right\rangle,$$

where $V = \sum_e V_e$ is the total volume of the group, $w^e = V_e/V$ is the specific volume of an element, and $\left\langle \varepsilon_v^e \right\rangle$ is the bulk strain averaged over an element:

$$\left\langle \varepsilon_v^e \right\rangle = \left\langle \varepsilon_1^e + \varepsilon_2^e + \varepsilon_3^e \right\rangle = \left\langle N(B_1 + B_2 + B_3)U \right\rangle$$
$$= \left\langle N \right\rangle (B_1 + B_2 + B_3)U \equiv \overline{B}_v U.$$

For a triangular prism, the value of the operator is

$$\overline{B}_v = \frac{1}{6}(B_1 + B_2 + B_3).$$

Now, to calculate the bulk rigidity matrix, we express the bulk strain energy through the node displacements:

$$H_v = \frac{\kappa}{2} V \langle \varepsilon_v \rangle^2 = \frac{\kappa}{2} V w^{eT} \left\langle \varepsilon_v^e \right\rangle^2 w^e = \frac{\kappa}{2} V U^T w^{eT} B_v^T B_v w^e U,$$

where κ is the bulk modulus. This yields $K_v^e = w^{eT} B_v^T B_v w^e$.

The bulk rigidity matrix constructed in this way provides a zero value of the average strain in the node vicinity. In this case, the volumetric locking is absent. The total rigidity matrix is calculated as the sum of shear and bulk rigidity matrices.

The damping matrix and the external force matrix are calculated by the formulas

$$C^e = \int_{\Omega^e} B^T G B d\Omega, \quad F^e = \int_{\Omega^e} N^T b d\Omega + \int_{\Gamma^e} N^T \hat{t} d\Gamma.$$

After constructing the global matrices with the use of the algorithm described above, we arrive at a system of linear differential equations in matrix form:

$$M\ddot{U} + C\dot{U} + KU = F. \tag{10}$$

System of equations (10) is solved numerically with the use of the Newmark scheme. We assume that u_n is the value of u at the instant $t = n\Delta t$, where Δt is the step in time. The relation between the quantities at a current time step and at the next one is given by the formulas

$$u_{n+1} = u_n + \Delta t \dot{u}_n + \frac{\Delta t^2}{2}\left[(1-\beta_2)\ddot{u}_n + \beta_2 \ddot{u}_{n+1}\right],$$
$$\dot{u}_{n+1} = \dot{u}_n + \Delta t\left[(1-\beta_1)\ddot{u}_n + \beta_1 \ddot{u}_{n+1}\right], \tag{11}$$

where $0 \le \beta_1, \beta_2 \le 1$ are the parameters determining the type of the difference scheme. Equations (11) give an explicit scheme when these parameters are zero; in the case of nonzero parameters, the scheme is implicit.

THE RANGE OF APPLICABILITY OF THE ONE-DIMENSIONAL MODEL

Figure 1b shows the calculated dependence of the first resonance frequency f_1 on the ratio of the resonator length to the resonator thickness, a/L, for a homogeneous resonator with a free upper boundary. The calculations were performed by the FEM. The frequency f_1 is normalized by the first resonance frequency f_{10} determined in [1] for the one-dimensional resonator. When the length of the resonator a is much greater than its thickness L, the first resonance is observed at the frequency f_{10} and the resonator is adequately described by the one-dimensional model. When $a \ge 4L$, the first resonance frequency deviates from f_{10} by no more than 4%. This ratio can conventionally be considered as the limit of applicability of the one-dimensional model. When the resonator length is smaller than $4L$, it is necessary to apply the FEM. For a cube with a free upper face ($a = L$), the resonance frequency is $f_1 = 0.78 f_{10}$, which corresponds to the result of measurement indicated by the square in Fig. 1b. The circle indicates the first resonance frequency ($f_1 = 0.98 f_{10}$) measured for a resonator with $a = 4.7L$ under a load in the form of a plate with a mass of 10.34 g. One can see that the result of measurement agrees well with the calculations performed by the FEM and by the formulas derived for the one-dimensional model. Calculations also showed that the resonance frequency is independent of the width-to-thickness ratio of the resonator b/L when $b \ge L$. For smaller values of b, no calculations were carried out. We note that, if, in our calculations, we fix the density of the upper plate, i.e., if we vary its mass in direct proportion to its length a, then, for a loaded resonator, we

obtain the dependence given in Fig. 1b. However, if we fix the mass of the upper plate, the resonance frequency will decrease still faster with decreasing ratio a/L.

DETERMINATION OF THE SIZE AND POSITION OF INHOMOGENEITIES FROM THE RESONANCE FREQUENCY SHIFT

From the practical point of view, it is of interest to consider the behavior of shear standing waves in a resonator with inhomogeneities of the shear modulus. We analyze the resonance characteristics for resonators with inhomogeneities in the form of a single inclusion in the resonator volume and in the form of a set of several similar inclusions positioned at different distances from the resonator boundaries. In hard inhomogeneities, the shear modulus exceeds the shear modulus of the resonator body; for soft inhomogeneities, the situation is reversed. We consider the limiting cases of soft inhomogeneities in the form of a liquid inclusion and an empty cavity. In both cases, the shear modulus is zero, but, for the liquid inclusion, the mass of the resonator remains approximately constant, because the density of the chosen liquid is chosen to be approximately identical to the density of the resonator material. In the presence of an empty cavity, the mass of the resonator decreases, which determines the difference between the two aforementioned cases. We note that, in all the cases, the size of inhomogeneities is much smaller than the wavelength.

Figure 2 shows the resonance curves calculated by the FEM near the first resonance for a resonator with the dimensions $L = 15$, $a = 70$, and $b = 40$ mm and with a load in the form of a plate with the mass $M = 19.5$ g. The inhomogeneity indicated by black color in the inset in Fig. 2 is at the center of the resonator and penetrates through the entire resonator width. The resonator was divided into 672 finite elements (FEs) with a height of 2.5 mm, a length of 5 mm, and a width of 10 mm. The inhomogeneity consisted of 32 elements and had the dimensions of a height of 5 mm (the size of two FEs), a length of 10 mm (two FEs), and a width of 40 mm (four FEs), which made up 4.76% of the resonator volume. In our calculations, we used the following parameters of the rubberlike material occupying the major part of the resonator volume: the density $\rho = 0.98$ g/cm^3, the Lame coefficients $\mu = 7.5$ kPa and $\lambda = 2.25 \times 10^7$ Pa, and the shear viscosity coefficient $\eta = 3.8$ Pa·s. The dashed line shows the resonance curve for a homogeneous resonator with reduced parameters. The first resonance frequency of the homogeneous resonator was 31.3 Hz, while the acceleration amplitude of the upper plate was 22 times greater than the acceleration amplitude of the lower plate of the resonator. Curve *1* was calculated for a resonator with an inhomogeneity in the form of a liquid-filled cavity with $\mu = 0$, $\eta = 0$, and $\rho = 1$ g/cm^3. In this case, the resonance frequency is smaller than that of

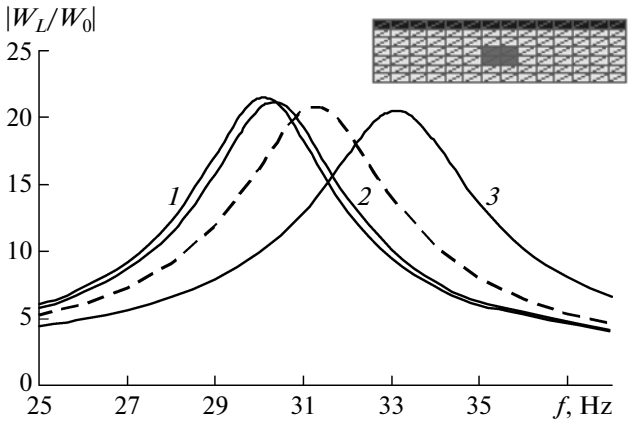

Fig. 2. Resonance curves calculated by the FEM for a resonator with an inhomogeneous inclusion (the solid lines) and for a homogeneous resonator (the dashed line): (*1*) a liquid-filled cavity, (*2*) an empty cavity, and (*3*) a solid inclusion with a shear modulus ten times greater than that of the resonator body.

the homogeneous resonator and comes to 30.1 Hz. Such a considerable difference (4%) allows detection of the inhomogeneity by the frequency shift. At the same time, to distinguish a liquid-filled cavity from an empty cavity, a more accurate frequency measurement is required. Resonance curve *2* was calculated for the resonator with an empty cavity ($\rho = 0$, $\mu = 0$, $\lambda = 0$, and $\eta = 0$). Here, the resonance frequency is 30.3 Hz, which is only 0.2 Hz greater than the value obtained for the resonator with the liquid inclusion. The method described in [1] allows one to measure the resonance frequency accurate to 0.1 Hz and, hence, to discriminate between liquid-filled and empty cavities. The presence of an inhomogeneity that is harder than the main material of the layer leads to an increase in the resonance frequency. Curve *3* was obtained for the case of an inhomogeneity the shear modulus of which was $\mu = 75$ kPa. In this case, the resonance frequency is 33.1 Hz.

Figure 3 shows the results of calculating the first resonance frequency of a resonator with the dimensions specified above and with several inhomogeneities in the form of empty cavities as a function of the relative volume of cavities. Each of the cavities penetrating through the resonator had the following dimensions: a height of 5 mm (two FEs), a length of 5 mm (one FE), and a width of 40 mm (four FEs), which made up 2.38% of the resonator volume. The inhomogeneities were positioned in a row at a constant height h; the number of cavities N in a row varied pairwise from 2 to 6 symmetrically about the axis passing through the resonator center. Hence, their relative volume increased from 4.76 to 14.28%. The numbers near the curves indicate the height of the position of cavity centers h in millimeters: at $h = 2.5$ mm, the cavities touch the lower plate of the resonator, and at $h = 12.5$ mm, they touch the upper plate. The parameters of the

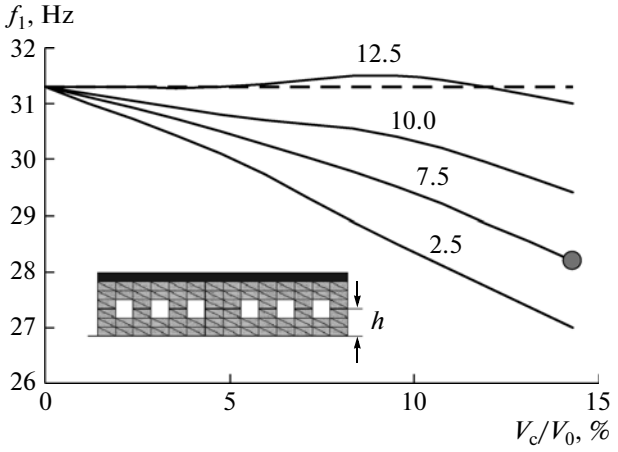

Fig. 3. Calculated dependences of the first resonance frequency on the relative volume of cavities for a resonator with inhomogeneities in the form of a horizontal row of empty cavities. The numbers near the curves indicate the height of the cavity center positions h in millimeters. The dashed line shows the first resonance frequency in a homogeneous resonator (31.3 Hz); the circle shows the measured frequency for a resonator with six cavities ($V_c/V_0 = 14.28\%$) positioned at the height $h = 7.5$ mm.

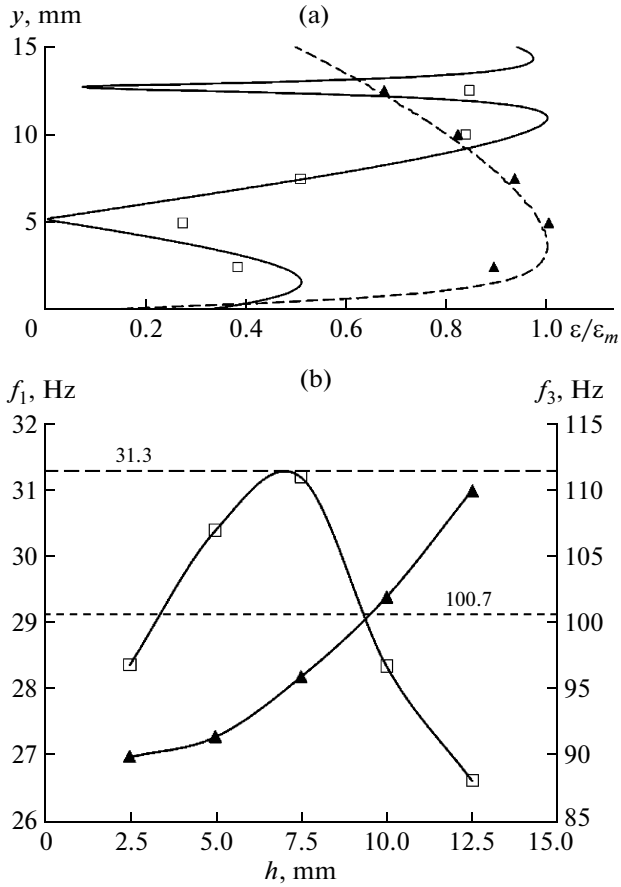

Fig. 4. (a) Distribution of shear strain throughout the resonator height at the first (the dashed line) and second (the solid line) resonance frequencies. The strain averaged over the cavity height is shown by triangles and squares for the first and second resonance frequencies, respectively. (b) Dependence of the first (triangles) and second (squares) resonance frequencies on the height of cavities position in the resonator. The number of cavities is $N = 6$.

rubberlike material had the aforementioned values: $\rho = 0.98$ g/cm^3, $\mu = 7.5$ kPa, $\lambda = 2.25 \times 10^7$ Pa, and $\eta = 3.8$ Pa·s. The dashed line shows the resonance frequency of a homogeneous resonator (31.3 Hz). The presence of cavities reduces the resonance frequency of vibrations. The maximal decrease in frequency is observed for the resonator with cavities positioned near its lower boundary (the curve corresponding to $h = 2.5$ mm). An increase in the number of cavities leads to a corresponding decrease in the resonance frequency. The presence of a small number of cavities ($N \leq 5$) immediately below the upper plate initially leads to a slight increase in the resonance frequency; however, from $N = 6$, the resonance frequency begins to decrease (the curve corresponding to $h = 12.5$ mm). A similar effect was qualitatively obtained for the one-dimensional model [2] with the resonator represented as a three-layer structure. The layer with cavities was represented in the form of a homogeneous layer with the effective elasticity and density calculated by the formulas $\mu_{\text{eff}} = \mu_0\left(1 - \frac{N}{14}\right)$ and $\rho_{\text{eff}} = \rho_0\left(1 - \frac{N}{14}\right)$, where μ_0 and ρ_0 are the elastic modulus and the density of the resonator material, respectively. The decrease in the resonance frequency in the resonator with cavities can be explained by the decrease in the effective elasticity of the resonator. The presence of cavities in the region with maximal shear strain leads to a more pronounced effect. In Fig. 4a, the dashed line shows the strain distribution throughout the height of the homogeneous resonator; the distribution was calculated from the standing wave profile at the first resonance frequency. The maximal strain is reached at a height of 4 mm above the lower boundary. The values of strain averaged over the cavity height are shown by triangles in Fig. 4a; these values are in qualitative agreement with the dashed curve. Near the upper boundary of the resonator, where the averaged strain is minimal, the resonance frequency weakly depends on the number of cavities. At the same time, in the maximal strain region near the lower boundary of the resonator, the dependence of the resonance frequency on the number of cavities is rather strong (see Fig. 3). In Fig. 4b, the triangles show the dependences of the first and second resonance frequencies on the height h for a resonator with six cavities. The first resonance frequency monotonically increases with the height of cavity positions and reaches its maximal value at $h = 12.5$ mm, i.e., when the cavities touch the upper plate. For the second resonance frequency, which is approximately three times as great as the first one, the averaged strain has a minimum at a height of approximately 5 mm (squares in Fig. 4a). Accordingly,

the dependence of the second resonance frequency on the height exhibits a different behavior (squares in Fig. 4b): the frequency increases, reaching its maximal value at $h = 7.5$ mm, and then decreases and reaches its minimal value when the cavities are at a height of 12.5 mm corresponding to maximal averaged strain. Note that the maximal value of the second resonance frequency at $h = 7.5$ mm is more than 10% greater than the frequency of the homogeneous resonator (100.7 Hz), which is indicated by the dashed line in Fig. 4b.

The measurements were performed for a resonator with inhomogeneities in the form of a row of six through cavities positioned at a height of 7.54 mm above the lower plate. The cavities had square cross sections and were constructed by placing steel bars in a casting form for plastisol at the required height. The casting form was filled with liquid plastisol heated to 177°C. After polymerization and cooling of plastisol to room temperature, the bars were removed. The resulting through cavities had identical square cross sections 5 mm on a side. The first resonance frequency (28.2 Hz) is shown by the circle in Fig. 3. It coincides with the frequency calculated for the inhomogeneity of this type and size to a high accuracy.

MEASUREMENTS IN A RESONATOR WITH AN IRREGULAR SHAPE

The finite-element method allows us to calculate the resonance curves for a resonator with an irregular shape. As an example, we used a resonator shaped as a parallelepiped with an approximately conical pit on one of its faces. Such shape defects may arise in the course of fabrication of an elastic resonator. The heated liquid polymer is poured in the casting form of necessary configuration; there, it polymerizes and becomes elastic. In the course of polymerization and cooling in the casting form with an open upper boundary, internal stresses arise in the polymer. These stresses lead to inhomogeneous shrinkage and to the appearance of a pit of an approximately conical shape with maximal depth at the center. The volume of the pit makes up 7–10% of the liquid polymer volume initially poured into the casting form.

The measurements were performed with a resonator in the form of a plastisol parallelepiped with the dimensions $36 \times 40 \times 40$ mm; the resonator was loaded with a plate with mass $M = 11$ g. One of the faces, with dimensions of 40×40 mm, had a pit of an irregular shape with a maximal depth of 4 mm near the face center. For measuring the profile of the pit, its surface was covered with thin aluminum foil, which was connected to one of the wires of a tester operating in the resistance measurement mode. The other wire of the tester was connected to a reference metal cone mounted on a micrometric feed. The contact between the cone and the foil was detected by the sound signal of the tester, after which depth measurement was performed. The cone moved along the pit at a varying step of 0.1–0.5 mm, depending on the degree of inhomogeneity of the profile. The diameter of the cone at the point of contact with the foils was 1 mm, which provided fair accuracy of profile measurement. The profile was measured in three cross sections at distances of 10, 20, and 30 mm from the edge. The dots in Fig. 5a show the results of measuring the profile of the pit in one of its cross sections. In numerical simulation, the resonator was divided into 1800 equilateral triangular prisms with a side of 4 mm. On one of the faces with dimensions of 40×40 mm, we outlined a region in the form of a rectangular parallelepiped with dimensions of $4 \times 32 \times 32$ mm, which contained 128 finite elements. All the elements of this region were assumed to have zero shear modulus and zero density. The pit profile used in the calculations is shown by a solid line in Fig. 5a. The volume of the pit used in the calculations (7.1%) was approximately the same as that of the actual pit.

In Fig. 5b, dots of different kinds show the measured resonance curves corresponding to different orientations of the face with the pit with respect to the direction of vibrations. The position of the face with the pit in the measurement of the corresponding resonance curve is indicated at the right of Fig. 5b. The arrows show the direction of vibrations. Curve *1* with the minimal resonance frequency (8.1 Hz) was obtained for the case of the pit position on the lateral face oriented perpendicularly to the vibration direction. The maximal value of the resonance frequency (10.3 Hz) was obtained when the face with the pit occupied the upper position (curve *4*). Curves *2* and *3* were measured with the pit on the bottom face and with the pit on the lateral face that was parallel to the vibration direction, respectively. From resonance curve *3*, we determined the values of the shear modulus (5 kPa) and shear viscosity coefficient (3 Pa · s) of the polymer. This was made with allowance for the fact that the resonance frequency only slightly depends on the resonator width. The aforementioned values of the shear modulus and the shear viscosity coefficient were used in calculating the resonance curves by the finite-element method (the solid lines in Fig. 5b). The small discrepancy between the measured and calculated curves can be explained by the inexact geometry of the model pit. To achieve better agreement, it is necessary to use a grid with finer elements, which requires much more computer time. It should be noted that the actual pit is asymmetric and, therefore, the measured values of the resonance frequency are somewhat different even for identical orientations of the face with the pit with respect to the vibration direction. For example, if we rotate the resonator with the pit on the upper face (position *4*) about the vertical axis, the resonance frequency will vary within 5%.

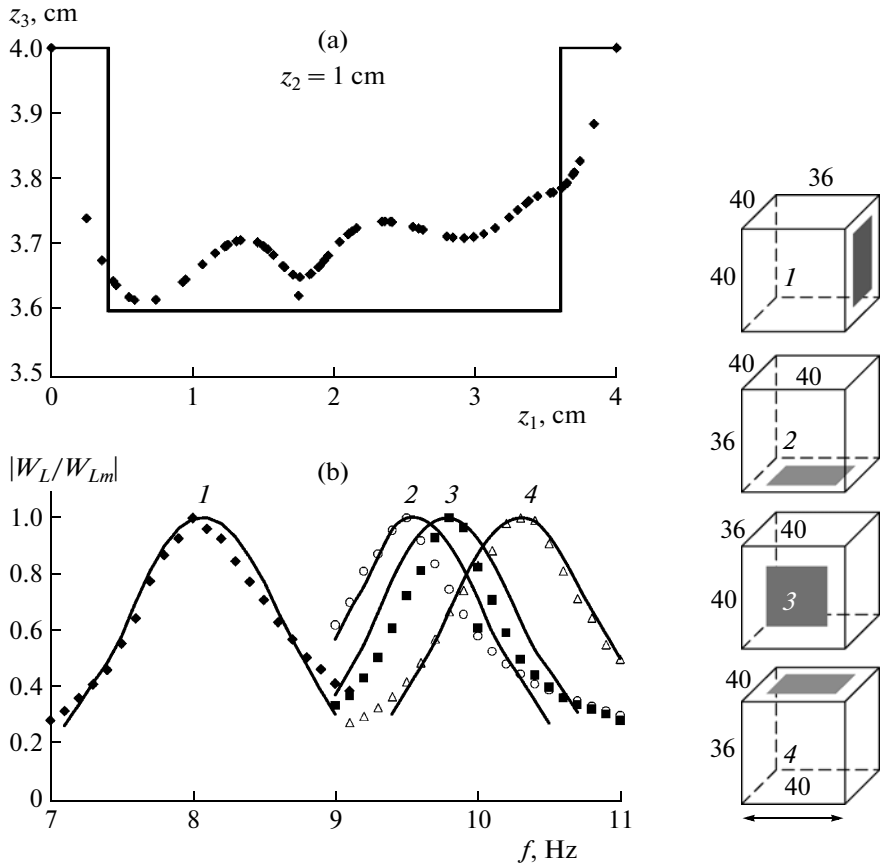

Fig. 5. (a) Profile of the pit in one of the cross sections. The dots represent the measured values, and the line shows the model representation. (b) Resonance curves obtained for a resonator in the form of a rectangular parallelepiped with a pit on one of its faces. The numbers near the curves correspond to different orientations of the face with the pit indicated by a grey color with respect to the vibration direction indicated by arrows. The results of calculations are shown by solid lines, and the experimental data by dots. The numbers near the ribs indicate their lengths in millimeters.

CONCLUSIONS

In our previous paper [1], we showed that, from the measurements of the resonance curves of a resonator made from rubberlike polymer, we can derive reliable information on the values of the shear modulus and the shear viscosity coefficient of the polymer in the low-frequency range. This, in its turn, allows us to determine the relaxation time spectrum and to construct an adequate rheological model of the polymer, which is important for determining its internal structure. In [2], this approach was applied to resonators with layered structures. However, the results obtained for them were based on the one-dimensional model with the resonator thickness being much smaller than the transverse resonator size. In measurements, we always deal with finite-size resonators; hence, it is necessary to determine the limits of applicability of the one-dimensional model. In the present paper, we showed that, if the thickness of a homogeneous resonator is four or more times smaller than its length, its resonance frequency varies within no more that 4%, which can be considered as the limit of applicability of the one-dimensional model. We note that the measurements described in [1] were performed with a resonator the thickness of which was five times smaller than its length; therefore, the results of calculations in terms of the one-dimensional model were in good agreement with experimental data.

Calculations for standing waves in a finite-size resonator were performed using the finite-element method modified for the case of incompressible media. The modification consisted in lifting the limitation concerning the volume conservation for an individual finite element under deformation. Instead, we required that the volume be conserved for a group of finite elements. This allowed us to avoid the volumetric locking. The computational algorithm was tested by the agreement between the results obtained from FEM calculations, the analytic results for a resonator in the form of a layer, and the experimental data. The FEM allows calculating the resonance characteristics of resonators with arbitrary shapes and with inhomogeneities of the shear modulus.

The modern methods of elastography of soft biological tissues solve the problem of determining the spatial distribution of shear modulus inhomogeneities from particle displacements under the effect of low-frequency vibrations. They mainly deal with inhomogeneities of the cyst type, which have the form of liquid-filled bubbles, or with solid tumors, which, as a rule, are harder than the surrounding healthy tissues. It is of interest to study the effect of such inhomogeneities on the resonance frequencies of a resonator. It was found that hard inclusions raise the resonance frequencies, whereas liquid-filled cavities reduce them. Empty cavities may both reduce and increase the resonance frequency, depending on their positions and relative volume. If a cavity is in the region of large shear strains, its presence reduces the resonance frequency, because the effective elasticity of the resonator is reduced. In the region of small strains, the decrease in elasticity is insignificant, while the effect of the decrease in the mass per unit length in the inhomogeneity region plays a more significant role, which leads to an increase in the resonance frequency. These effects were demonstrated for the first and second resonance frequencies, at which the spatial distributions of shear strain are different. In particular, when the cavities are near the upper plate, the value of the first resonance frequency may be higher than that of a homogeneous resonator without cavities, whereas the value of the second resonance frequency may be lower than the corresponding value for the homogeneous resonator.

The efficiency of the modified finite-element method was demonstrated by the example of calculating the resonance curves for a resonator with an irregular shape. The resonator had the form of a rectangular parallelepiped with a pit on one of its faces. The relative volume of the pit made up 7% of the resonator volume, and its profile was asymmetric. In calculations, we used the values of shear elasticity obtained from the resonance curve, which was measured with the pit position on the face parallel to the vibration direction. The presence of the pit on this face leads to variation of the resonator width. However, our calculations showed that the resonance frequency weakly depends on the resonator width. Therefore, we assumed that the influence of width variation due to the pit presence on frequency is rather small. The shear modulus was calculated for a resonator in the form of a rectangular parallelepiped without a pit. The comparison between the measured resonance curves and the calculated ones showed their good agreement, which justified the aforementioned approach. As in the case of the inhomogeneity in the form of a row of cavities, the resonance frequency is higher when the cavities occupy the upper position and lower when the cavities are at the bottom. This result agrees well with the explanation proposed above for the dependence of the resonance frequency on the cavity position with respect to the strain antinode or node in a shear standing wave. From the resonance curve measurements at multiple resonance frequencies, it is possible to determine the height at which a cavity-type inhomogeneity is positioned. This may be done with higher accuracy if we smoothly vary the resonance frequencies by varying the mass of the upper plate [1].

ACKNOWLEDGMENTS

This work was supported by the Russian Foundation for Basic Research (project no. 08-02-00368) and the Presidential Program in Support of the Leading Scientific Schools of Russia (grant no. NSh-4590.2010.2).

REFERENCES

1. V. G. Andreev, T. B. Krit, and O. A. Sapozhnikov, Akust. Zh. **56**, 190 (2010) [Acoust. Phys. **56**, 168 (2010)].
2. V. G. Andreev, T. B. Krit, and O. A. Sapozhnikov, Akust. Zh. **56**, 579 (2010) [Acoust. Phys. **56**, 605 (2010)].
3. T. J. R. Hughes, *The Finite Element Method* (Prentice Hall, Englewood Cliffs, 1987).
4. O. C. Zienkiewicz and L. R. Taylor, *The Finite Element Method* (Butterworth-Heinemann, London, 2000).
5. R. W. Bell, G. T. Houlsby, and H. J. Burd, Commun. Num. Methods Eng. **9**, 313 (1993).
6. J. R. Joldes, A. Wittek, and K. Miller, Proc. MICCAI, No. 1, 54 (2006).

Translated by E. Golyamina